NASA TECHNICAL MEMORANDUM

NASA TM X-73462

NASA TM X-73462

(NASA-TM-X-73462) FAILURE MECHANICS OF FIBER COMPOSITE NOTCHED CHARPY SPECIMENS (NASA) 24 p HC $3.50 CSCL 11D

N76-30295

Unclas
G3/24 49569

FAILURE MECHANICS OF FIBER COMPOSITE NOTCHED CHARPY SPECIMENS

by C. C. Chamis
Lewis Research Center
Cleveland, Ohio 44135

TECHNICAL PAPER to be presented at
the Army Symposium on Solid Mechanics:
Composite Materials - The Influence of
Mechanics of Failure on Design
Cape Cod, Massachusetts, September 14-16, 1976

FAILURE MECHANICS OF FIBER COMPOSITE NOTCHED CHARPY SPECIMENS

C. C. Chamis
Lewis Research Center
Cleveland, Ohio

ABSTRACT

A finite element stress analysis was performed to determine the stress variation in the vicinity of the notch and far field of fiber composites Charpy specimens (ASTM Standard). NASTRAN was used for the finite element analysis assuming linear behavior and equivalent static load. The unidirectional composites investigated ranged from T75/E to S-Glass/E with the fiber direction parallel to the long dimension of the specimen. The results indicate a biaxial stress state exists in (1) the notch vicinity which is dominated by transverse tensile and interlaminar shear and (2) near the load application point which is dominated by transverse compression and interlaminar shear The results also lead to the postulation of hypotheses for the predominant failure modes, the fracture initiation, and the fracture process. Finally, the results indicate that the notched Charpy test specimen is not suitable for assessing the impact resistance of nonmetallic fiber composites directly.

INTRODUCTION

The notched Charpy test method has been used extensively to assess the impact resistance and the notch sensitivity of unidirectional composites under impact load. The use of the notched Charpy test method for assessing composite impact resistance has three attractive features: (1) simplicity, (2) established test procedures (ASTM Standard E23-73), and (3) commonality with a successful method for assessing conventional metal notch sensitivity. However, the geometry and load application of the notched Charpy composite test specimen are such that the specimen is in a biaxial stress state and is loaded primarily in short beam shear (interlaminar shear stress). This type of load and the relatively low shear strength of unidirectional composites results in a high probability of interlaminar shear stress failures. This type of failure does not fracture fibers which provide the maximum impact resistance and, therefore, the test may not be suitable for assessing impacting resistance in nonmetallic fiber composites.

Although the notched Charpy test specimen has been used for years in testing metals and recently in testing composites, no analysis has been performed to determine the detailed stress state variation in the notch vicinity. In general, the physical problem of the notched Charpy test specimen is dynamic and nonlinear; solution of this problem is difficult. However, a good first order approximation may be obtained by determining the stress variation in the notch vicinity by assuming linear behavior and an equivalent static load. The detailed stress variation near the notch obtained from such a solution should help provide insight and possible identification of predominant fracture modes, fracture initiation, and fracture processes. Therefore, it is the objective of this investigation to carry out a detailed stress analysis using NASTRAN to determine the stress variation in the notch vicinity of the notched Charpy composite test specimen assuming linear behavior and equivalent static load.

The type of analysis performed, the results obtained, and the interpretation of these results relative to fracture modes, fracture initiation, and fracture process of the notched Charpy composite test specimen and its utility in assessing composite impact resistance are described herein.

ANALYSIS

The specimen geometry, the finite element representation, the finite element analysis method, and the composite systems analyzed are described in this section.

Specimen Geometry

The geometry of the Charpy test specimen (ASTM STD E23-7) is depicted in figure 1. As can be seen in this figure, the overall length of the specimen is 2.164 inches and the length between supports is 1.574 inches. The specimen width is 0.394 inch. The specimen unnotched depth is 0.394 inch and the depth at the notch is 0.315 inch. The notch is 0.079 inch deep and has a 45° opening symmetric about the specimen midlength.

Finite Element Representation

The specimen is assumed to be symmetric with respect to both geometry and loading about its midlength for analysis purposes. The material properties are uniform, orthotropic, and obey a linear stress strain law throughout the analysis. In addition, the specimen is assumed to be in a state of plane stress. That is, the stresses are permitted to vary along the specimen length and through the thickness but

not through the width. This reduces the stresses to be calculated to three, two normal and one shear.

With these assumptions, plane stress finite elements can be used to model the Charpy test specimen and only one-half of its length need be used in the finite element representation. The finite element representation of the specimen and the boundary conditions prescribed are shown in figure 2. As can be seen in this figure, all of the elements are quadrilateral except for one triangular element at the notch. Note that the displacement boundary conditions do not permit displacements in the x direction at the line of symmetry ($x = 0$) and y displacements at the support points. The specimen is assumed to be subjected to static concentrated load at its midlength.

The statistics of the finite element representation are as follows:

Number of nodes or grid points	197
Number of displacement degrees of freedom (DOF) (2 degrees of freedom per node)	394
Number of elements	168
DOF eliminated using the boundary conditions (7 from $u = 0$ and 1 from $v = 0$)	8
Number of free DOF (394-8)	386

Finite Element Analysis Method

The NASTRAN general purpose structural analysis finite element computer program was used for the finite element analysis method. The specific elements used are identified as CQDMEM and CTRMEM in the NASTRAN library-resident elements. The triangular element is a constant strain plane element and the quadrilateral combines four triangular elements, the stiffness of which is generated using the four constant strain triangular elements internally in NASTRAN together with the appropriate anisotropic material properties. NASTRAN obtains the solution using a displacement formulation via rigid format 1. Only one-half of the concentrated load is needed with the half-length of the specimen modeled in the finite element representation.

Composite Systems Analyzed

Charpy test specimens made from six different composite systems were analyzed. Namely: Thornel 75/epoxy (T75/E), Modmor I/epoxy (MOD I/E), boron/epoxy (B/E), Modmor II/epoxy (MOD II/E), Kevlar 49/E (KEV 49/E), and S-glass/epoxy (S-G/E). The specimens were all unidirectional composites with the fibers parallel to the length (x-axis, fig. 1) of the specimen.

The composite systems listed were selected because characterization data and Charpy test data for these composites were reported in reference 1. Tensile and shear fracture stress ranges of these composites reported in reference 1 are summarized in table I. Typical values for compression fracture stresses and Poisson's ratios are shown in table II. The plane stress-strain relationship (stiffness) coefficients required for input to NASTRAN are summarized in table III. The values in table III were obtained from the moduli data reported in reference 1 and the Poisson's ratio values shown in table II for these composite systems.

The relationships between the NASTRAN stiffness coefficients (G's), and the usual engineering constants are:

$$G_{11} = E_{\ell 11}/(1 - \nu_{\ell 12}\nu_{\ell 21}) \tag{1}$$

$$G_{12} = \nu_{\ell 21}G_{11} = \nu_{\ell 12}G_{22} = G_{21} \tag{2}$$

$$G_{22} = E_{\ell 22}/(1 - \nu_{\ell 12}\nu_{\ell 21}) \tag{3}$$

$$G_{33} = G_{\ell 12} \tag{4}$$

The notation in equations (1) to (4) is as follows: $E_{\ell 11}$ denotes the longitudinal modulus, $E_{\ell 22}$ the transvers modulus, $G_{\ell 12}$ the shear modulus, $\nu_{\ell 12}$ the major Poisson's, and $\nu_{\ell 21}$ the minor Poisson's ratios. For an elastic material, the two Poisson's ratios are related by the well known relation.

$$\nu_{\ell 21} = \nu_{\ell 12}E_{\ell 22}/E_{\ell 11} \tag{5}$$

RESULTS AND DISCUSSION

The load conditions used for the analysis and the various stress results obtained are described in this section. The stress results include: (1) stress variation in the notch vicinity and comparisons with those predicted by simple beam theory; (2) typical interlaminar shear stress contours; and (3) typical bearing stress variation near the support.

Load Conditions

Two sets of loads were used in determining stress variations near the notch. The

first set of loads was selected to produce fracture in the specimen under an equivalent static load. The stress state generated from this load can then be compared to the fracture stress of the composite. The procedure for selecting this load is as follows:

1. Assume the longitudinal tensile stress at the notch root produces fracture.
2. Use the simple beam formula

$$P = (bh^2/6\ell)S_{\ell 11T} \tag{6}$$

where P is the load used for the NASTRAN stress analysis; b is the specimen width and is equal to 0.394 inch; h is the specimen thickness at the root and is equal to 0.315 inch; ℓ is the specimen length to the edge of the support and is equal to 0.787 inch; and $S_{\ell 11T}$ is the longitudinal tensile-fracture stress of the composite.

Substituting these numerical values in equation (6) yields

$$P = 0.00828\ S_{\ell 11T} \tag{7}$$

3. Substitute for $S_{\ell 11T}$ in equation (7) the longitudinal fracture stress from table I. The results for the composite systems investigated (rounded to the nearest "5") are: (stress variations for other loads are obtained by direct ratio).

Composite system	Equivalent static fracture load, lb	Value selected from table I
T75/E	1275	High value
MOD I/E	1070	Low value
B/E	1770	Average
MOD II/E	1270	Average
KEV 49/E	1340	Average
S-G/E	1810	Average

The second load set was assumed to be constant (1320 lb) for all composite specimens. This constant load was selected in order to compare the stress state variation near the notch root and thereby assess the influence of the different composite systems.

Stress Variation in the Notch Vicinity

The stress variation produced by the equivalent static fracture load for T75/E is plotted in figure 3 (a - longitudinal; b - transverse; c - shear). In this and subsequent figures the specimen depth is plotted as ordinate and the stress magnitude as abscissa. Each stress is plotted at three different span sections near the notch vicinity denoted by $x = 0.025$, 0.075, and 0.125 inch, respectively. The notch root is at $x = 0$ (fig. 2).

Both the composite transverse fracture stresses tensile (low value (table I) and compression (table II)) are shown in figure 3(b). The interlaminar shear fracture stress is shown in figure 3(c). The corresponding longitudinal fracture stresses are not shown because they are beyond the scale of figure 3(a).

The important points to be observed from the calculated results in figure 3 on a comparative basis and in conjunction with the data from tables I and II are:

1. The longitudinal stress (fig. 3(a)) near the notch root is tensile and is about 50 percent of the corresponding fracture stress (72 ksi compared to 142 ksi, low value table I). This relatively low longitudinal tensile stress will not produce fiber fractures.

2. Longitudinal tensile stress (fig. 3(a)) of considerable magnitude is present in the notch vicinity below the notch root line.

3. The transverse stress (fig. 3(b)) is tensile in the notch root vicinity and exceeds the composite corresponding fracture stress.

4. Relatively high longitudinal compressive stresses are present near the load application point (fig. 3(a)) (140 ksi versus approximately 130 ksi for the corresponding fracture stresses).

5. The transverse stress (fig. 3(b)) is compressive near the load application point and its magnitude exceeds the corresponding composite fracture stress.

6. The interlaminar shear stress has magnitudes which exceed the corresponding fracture stress below and above the notch line and especially near the load application point (fig. 3(c)).

The high compressive stresses near the load application point, the high transverse tensile stress near the notch root, the interlaminar shear stress sign reversal, and the large magnitude of the interlaminar shear stress are not intuitively obvious results from simple beam theory.

The important conclusion from the above observations is that the equivalent static load is sufficient to cause fracture near the notch root and near the load application point. Near the notch root the critical stresses are transverse tensile and interlaminar shear. Near the load application point the critical stresses are transverse com-

pression and interlaminar shear. Both of these combinations are likely to produce local delaminations prior to fiber fractures.

The stress variations near the notch root and near the load application points corresponding to figure 3 are shown in figure 4 for MOD I/E, in figure 5 for KEV 49/E, and in figure 6 for S-G/E. The corresponding fracture stresses are shown in a similar manner as in figure 3. Though stress variations are not shown here, those for B/E are similar to MOD I/E and those for type A/E are similar to MOD II/E.

As can be observed from the plots in figures 4 to 6 the stress variations are similar to corresponding ones in figure 3. It is important to observe, however, the large stresses (longitudinal compression, transverse compression, and intralaminar shear) in the KEV 49/E specimen (fig. 5) relative to the corresponding fracture stresses. Based on the conclusions following the discussion of the results in figure 3, the KEV 49/E specimen would probably start delaminating at very low values of the equivalent static load. Observe, also, the relatively high stresses in the S-G/E specimen (fig. 6) for transverse compression and interlaminar shear compared to corresponding fracture stresses. This specimen, too, will probably start delaminating at low values of the equivalent static load.

Interlaminar Shear Stress Contours

It was noted in the previous discussion that the interlaminar shear stress is important in initiating fracture by delamination in Charpy composite specimens. It is of interest, therefore, to see the variation of this stress through the thickness and along the length of the specimen. Such a variation is best illustrated graphically by stress contour plots.

The interlaminar shear stress contour plot for KEV 49/E is shown in figure 7. Peak values are noted with an asterisk in this figure. As can be observed in figure 7 the interlaminar shear stresses are relatively high compared to the corresponding fracture stress of 6.8 ksi from table I. A possible conclusion from this observation is that once delamination is initiated it is probably driven subsequently by the high interlaminar shear stress present through the whole length of the specimen.

Interlaminar shear stress contour plots for the other specimens are similar to that of the KEV 49/E and are not shown here. The magnitudes of the stress contours depend on the load. However, the observations and conclusions are the same as those already made for the KEV 49/E specimen.

Comparisons with Simple Beam Theory

Stress variations in the notch vicinity predicted by the finite elemen stress analysis for the composite specimens investigated and for the same load are compared with those predicted using simple beam theory. Stress variation based on both full and reduced sections are calculated using the simple beam theory.

Comparison results for the longitudinal stress are presented in figure 8 for two vertical sections: $x = 0.025$ inch, figure 8(a) and $x = 0.075$ inch, figure 8(b). In this figure, the stress variations predicted by the simple beam theory equation

$$\sigma_x = 12\ P(0.787 - x)3/bh^2 \tag{8}$$

are shown by straight lines for both the full and reduced sections. The important points to be observed from the results in figure 8 are:

1. The longitudinal stress variation predicted by the finite element is approximately the same for all the composite systems.

2. The simple beam theory predicts stress variations, relative to those of the finite element, which are:

   a. Unconservative above the notch root when the full section is used.

   b. Conservative below the neutral plane and near the top when the reduced section is used.

The conclusion from the above observations is that simple beam theory predicts longitudinal stress variations in the notch vicinity of Charpy specimens which are in considerable error (as much as 100 percent) when compared to finite element results, and this theory is therefore inadequate to predict these stresses.

Comparison results for the interlaminar shear stress are presented in figure 9 for two vertical sections: $x = 0.025$ inch in figure 9(a), and $x = 0.125$ inch in figure 9(b). Note in these figures the stress variations predicted by the simple beam theory equation

$$\tau_{xy} = \frac{1.5\ P}{bh}\left[1 - \left(\frac{2y}{h}\right)^2\right] \tag{9}$$

using the reduced section only, are shown as parabolas. The important points to be observed from the results in figure 9 are:

1. The interlaminar shear variation nearest the notch ($x = 0.025$ in. or less than the notch depth, fig. 2), depends on the composite system, and appears to be inversely

proportional to the ratio G_{11}/G_{22} table III, also $E_{\ell 11}/E_{\ell 22}$ as may be deduced from equations (1) and (3).

2. The simple beam theory does not predict the interlaminar shear stress variation near the notch at sections closer than the notch depth.

3. The interlaminar shear stress variation appears to be insensitive to composite system at sections which are beyond 1.5 times the notch depth (fig. 9(b)).

4. The simple beam theory predicts interlaminar shear stress variations above the notch root which are comparable to those predicted by the finite element analysis at sections which are beyond 1.5 times the notch depth (fig. 9(b)).

The conclusion from the above observations is that simple beam theory with reduced section can be used to predict the interlaminar shear stress variation at sections which are 1.5 times the notch depth beyond the notch.

Comparison results for the transverse, or through-the-thickness normal stress (y-direction, fig. 2) variations for the various composites are presented in figure 10 for one vertical section (x = 0.025 in.). As can be seen in this figure, this normal stress near the notch root depends on the composite system. The magnitude of this normal stress appears to be inversely proportional to the orthotropy ($E_{\ell 11}/E_{\ell 22}$) ratio as was the case for the interlaminar shear stress. No comparisons with simple beam theory are shown because the simple beam theory does not predict this stress. The following observations are worthy of note from figure 10:

1. The transverse, or through-the-thickess normal stress (y-direction, fig. 2) is insensitive to composite system above the neutral plane (above specimen depth 0.24 in.).

2. The transverse, or through-the-thickness normal stress (y-direction, fig. 2) approaches large compressive magnitudes near the load application point and probably starts inducing local failures at relatively low load values.

Bearing Stresses Near Support

Typical bearing stress variations through the depth near the support are shown in figure 11 for Charpy composite test specimens. The bearing stress variations are shown in figure 11(a) for the three sections noted in the schematic in figure 11(b).

It can be seen in figure 11(a) that the bearing stress is very high near the support and decays rapidly through the depth and away from the support. The bearing stress near the support is of sufficient magnitude to produce local damage in some composites. This is readily established by comparing the transverse compression fracture stress from table II with curve A (fig. 11(a)). The local damage near the end support will most likely be a local indentation which will contribute to the lateral displacement

(y-direction, fig. 2) at the beam midlength. It is important to note that simple beam theory does not predict either the local damage near the support or its contribution to the lateral displacement.

The important conclusion from the previous discussion is that the bearing stresses near the support are of sufficient magnitude to produce local damage in Charpy composite test specimens.

FRACTURE MODES

The previous discussion dealing with the stress variations near the notch of Charpy composite test specimens leads to the following hypotheses for fracture modes, fracture initiation, and fracture process in nonmetallic fiber composites.

Fracture Modes

The hypotheses for predominant fracture modes are:

1. Interlaminar shear below the notch root
2. Transverse tension combined with interlaminar shear at the notch root and followed by possible fiber fractures
3. Transverse compression combined with interlaminar shear and longitudinal compression near the load application point
4. Interlaminar shear near the specimen center

Fracture Initiation

The hypothesis for fracture initiation in Charpy composite test specimens is as follows:

1. Near the notch root, fracture initiates when a combination of transverse tensile and interlaminar shear exceed their corresponding fracture stresses (critical values).

2. Near the load application point, fracture initiates when a combination of transverse compression, interlaminar shear, and longitudinal compression exceeds the corresponding fracture stresses.

3. Near the specimen center, fracture initiates when the interlaminar shear stress exceeds the corresponding fracture stress.

It is important to note that fracture may initiate sequentially or simultaneously in the three locations described above. A nonlinear analysis is required to determine the sequence of fracture initiation at these three locations.

Fracture Process

The hypothesis for the fracture process in the Charpy composite test specimen is as follows:

1. The high interlaminar shear stresses cause delamination and thus free surfaces near the notch root and near the load application point.

2. The delaminated surfaces reduce the specimen section to progressively thinner sections. Each delaminated thin section acts as an independent thin beam and continues to carry load in flexure.

3. The process continues, probably simultaneously, from both top and bottom towards the center until the specimen fractures completely either by delamination or fiber fractures or possible combinations of both.

It is noted at this juncture that direct proof of the above three hypotheses would require nonlinear and detailed fractographic analyses both of which are <u>not</u> part of this investigation's objectives.

A logical conclusion from the discussion of the above hypotheses and the results of the detailed stress analysis is that the notched Charpy test method is not suitable to assess the impact resistance of nonmetallic fiber composites directly. Its most serious drawback is that the predominant initial failure modes are combinations of transverse tensile or compression with interlaminar shear. Neither of these modes stresses the composite to its maximum efficienty which is only achieved when fiber fracture occurs.

SUMMARY OF RESULTS AND CONCLUSIONS

The major results of the NASTRAN linear stress analysis of ASTM notched Charpy unidirectional composite test specimens are as follows:

1. The critical stresses near the notch root are transverse tension and interlaminar shear.

2. The critical stresses near the load application point are transverse compression and interlaminar shear.

3. The simple beam theory is not adequate to predict longitudinal and interlaminar shear stresses near the notch. However, this theory may be used to predict the interlaminar shear stress at sections beyond 1.5 times the notch depth.

4. Both the interlaminar shear stress and the transverse tensile stress variations near the notch root depend on the composite system. Their magnitudes appear to be inversely proportional to the orthotropy ratios (E_{f11}/E_{f22}) for the same load.

5. The bearing stresses have high magnitudes near the support point and may cause local damage possibly in the form of indentation. These stresses decay rapidly away from the support and appear to be independent of the composite system.

6. The hypotheses formulated for fracture modes, fracture initiation, and fracture process are as follows: The dominant fracture modes are transverse tension, transverse compression, and interlaminar shear. Fracture initiates when combinations of these stresses reach critical values. The interlaminar shear stress causes free surfaces via delaminations which tend to reduce the specimen to thinner flexural type specimens. The process continues until the specimen fractures completely either by delamination, or fiber fracture, or possible combination of both.

7. The notched Charpy test method is not suitable for assessing the impact resistance of nonmetallic fiber composites directly.

REFERENCE

1. Friedrich, L. A. and Preston, J. L., Jr., "Impact Resistance of Fiber Composite Blades Used in Aircraft Turbine Engines," PWA-4727, May 1973; also NASA CR-134502.

TABLE I. - MEASURED FRACTURE STRESS RANGES (KSI) (REF. 1)

Composite system	Longitudinal tensile		Transverse tensile		Interlaminar shear			
					Short beam		Torsional rod	
	High	Low	High	Low	High	Low	High	Low
Thornel 75/epoxy (T75/E)	154	142	4.5	3.8	7.8	7.8	7.3	7.0
Modmore I/epoxy (MOD I/E)	146	129	5.1	5.0	8.4	8.2	7.2	6.8
Boron/epoxy (B/E)	222	205	9.3	7.2	15.3	14.7	13.2	12.8
Modmore II/epoxy (MOD II/E)	161	146	6.0	5.8	10.3	9.4	10.8	10.0
Kevlar 49/epoxy (KEV 49/E)	170	154	3.7	2.4	6.9	6.8	5.0	4.0
S-glass/Epoxy (S-G/E)	222	216	14.0	12.0	14.0	12.6	17.1	16.7

TABLE II. - TYPICAL COMPRESSION FRACTURE STRESSES AND POISSON'S RATIO

Composite system	Compression fracture stress		Poisson's ratio
	Longitudinal (ksi)	Transverse (ksi)	
T75/E	130	20	0.36
MOD I/E	128	28	.34
B/E	232	18	.41
MOD II/E	180	30	.35
KEV 49/E	42	9	.46
S-G/E	110	25	.36

TABLE III. - NASTRAN PLANE STRESS-STRAIN RELATIONSHIPS

Composite system	Stress-strain coefficient (10^6 psi)				Orthotropy ratio, G_{11}/G_{22}
	G_{11}	$G_{11} = G_{12}$	G_{22}	G_{33}	
T75/E	38.0	0.41	1.16	0.63	33
MOD I/E	30.6	.40	1.17	.70	26
B/E	30.6	2.10	5.14	1.95	6
MOD II/E	19.4	.40	1.13	.59	17
KEV 49/E	11.5	.39	.85	.39	14
S-C/E	8.79	1.17	3.26	1.27	3

$$\begin{Bmatrix} \sigma_x \\ \sigma_y \\ \sigma_{xy} \end{Bmatrix} = \begin{bmatrix} G_{11} & G_{12} & 0 \\ G_{21} & G_{22} & 0 \\ 0 & 0 & G_{33} \end{bmatrix} \begin{Bmatrix} \epsilon_x \\ \epsilon_y \\ \epsilon_{xy} \end{Bmatrix}$$

(For orthotropic material)

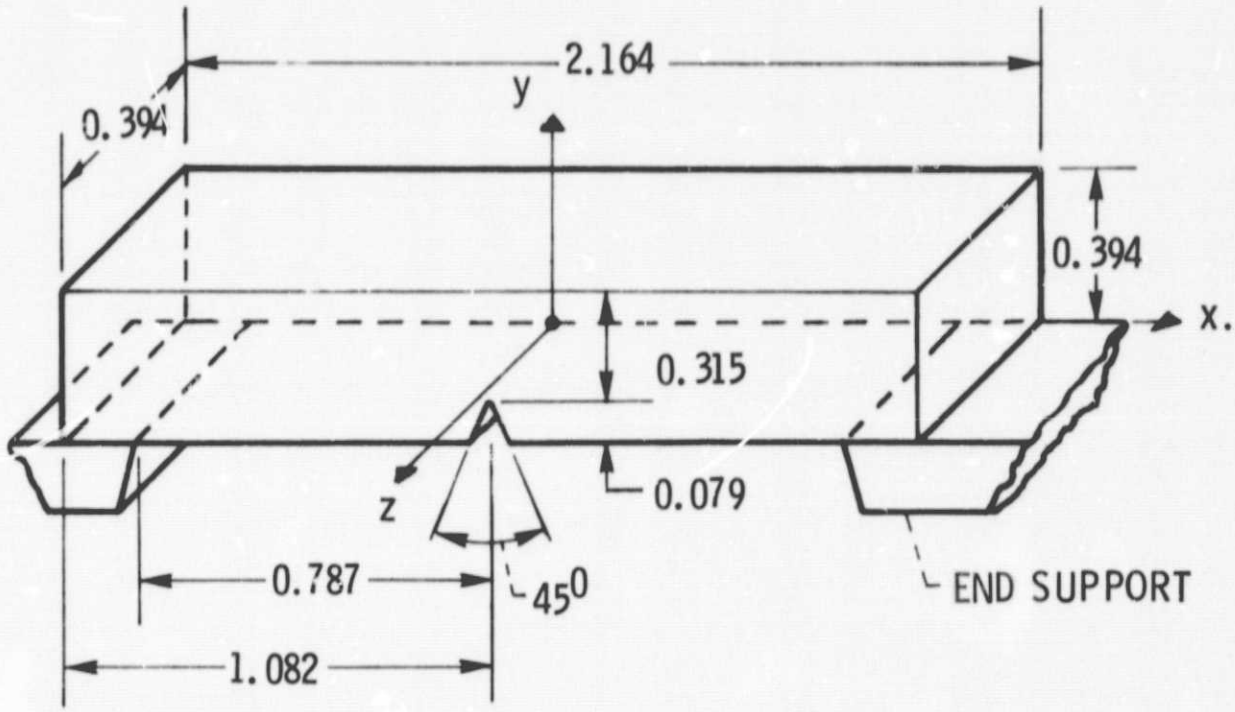

Figure 1. - Geometry of ASTM Charpy test specimen.
(All dimensions in inches.)

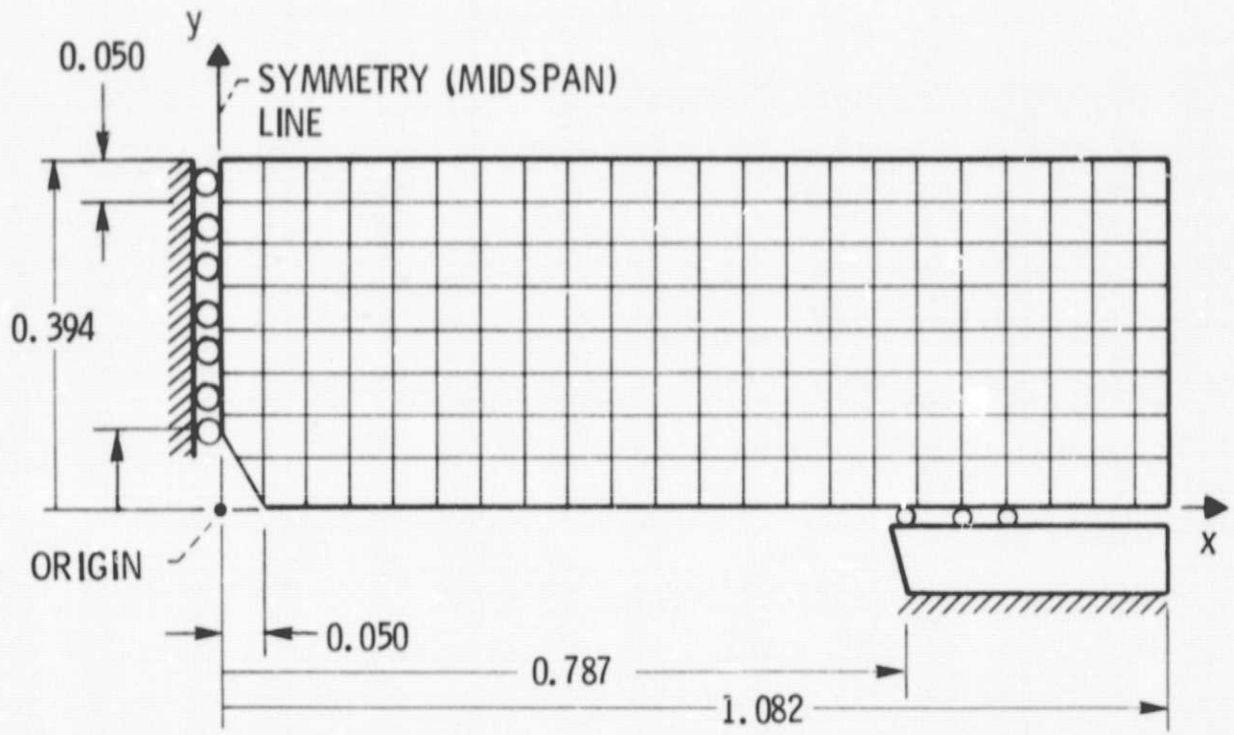

FINITE ELEMENT STATISTICS:

NODES	197
D.O.F./NODE	2
ELEMENTS	168
B.C's	u = 0 AT SYM. LINE; v = 0 AT x = 0.787 AND y = 0
MATERIAL	ORTHOTROPIC, FIBERS PARALLEL TO X-AXIS
LOAD POINT	x = 0; y = 0.394

Figure 2. - ASTM Charpy test specimen - finite element representation.

(All dimensions in inches.)

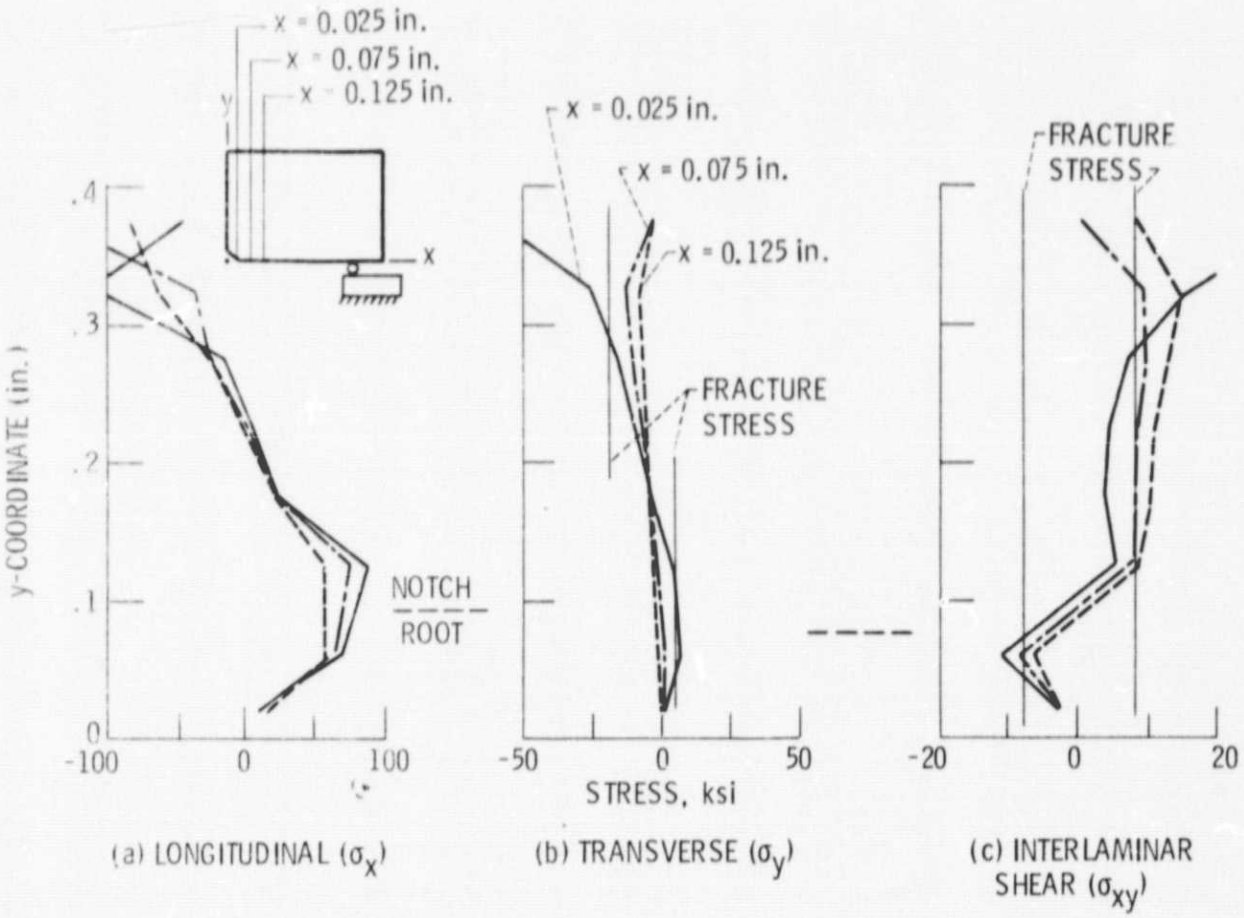

Figure 3. - T75/E ASTM Charpy test specimen: variation of stresses at sections in the vicinity of notch (static load = 1275 lb).

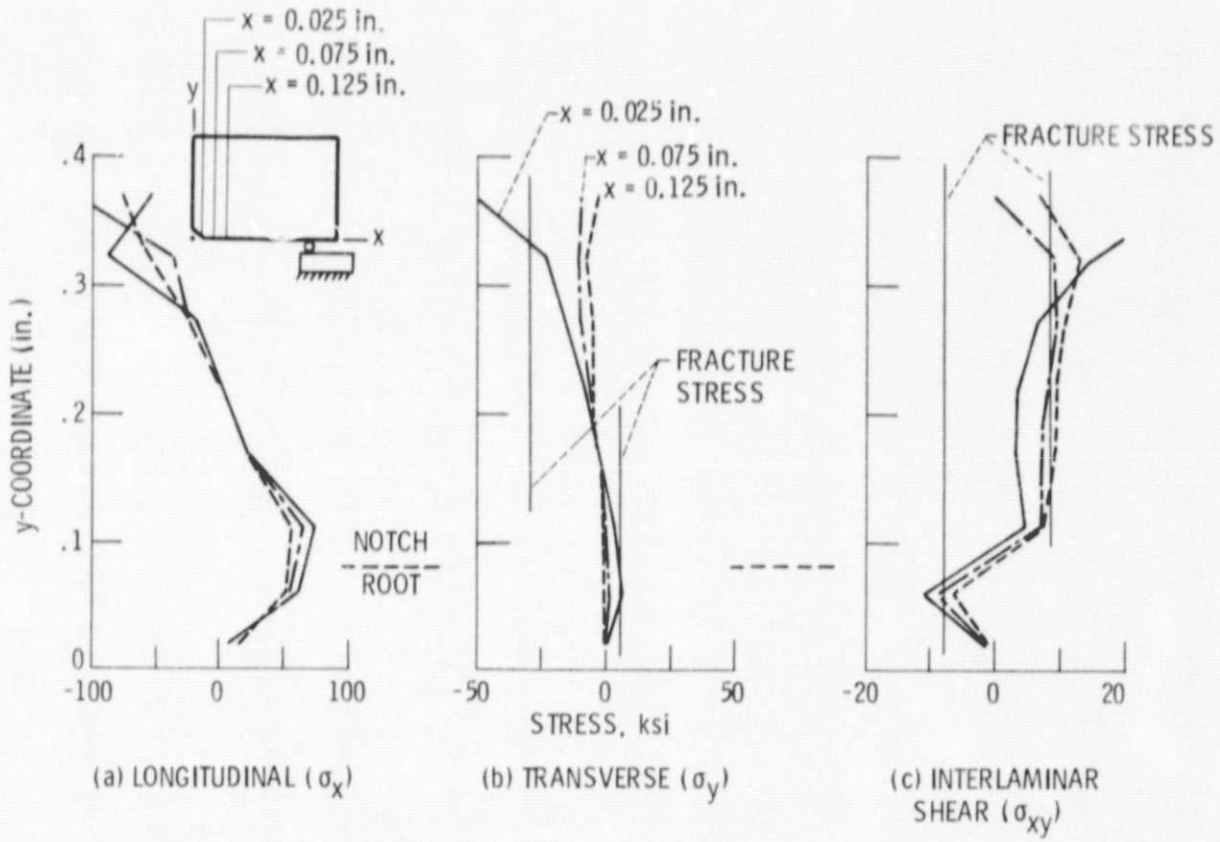

Figure 4. - Mod I/E ASTM Charpy test specimen: variation of stresses at sections in the vicinity of notch (static load = 2152 lb).

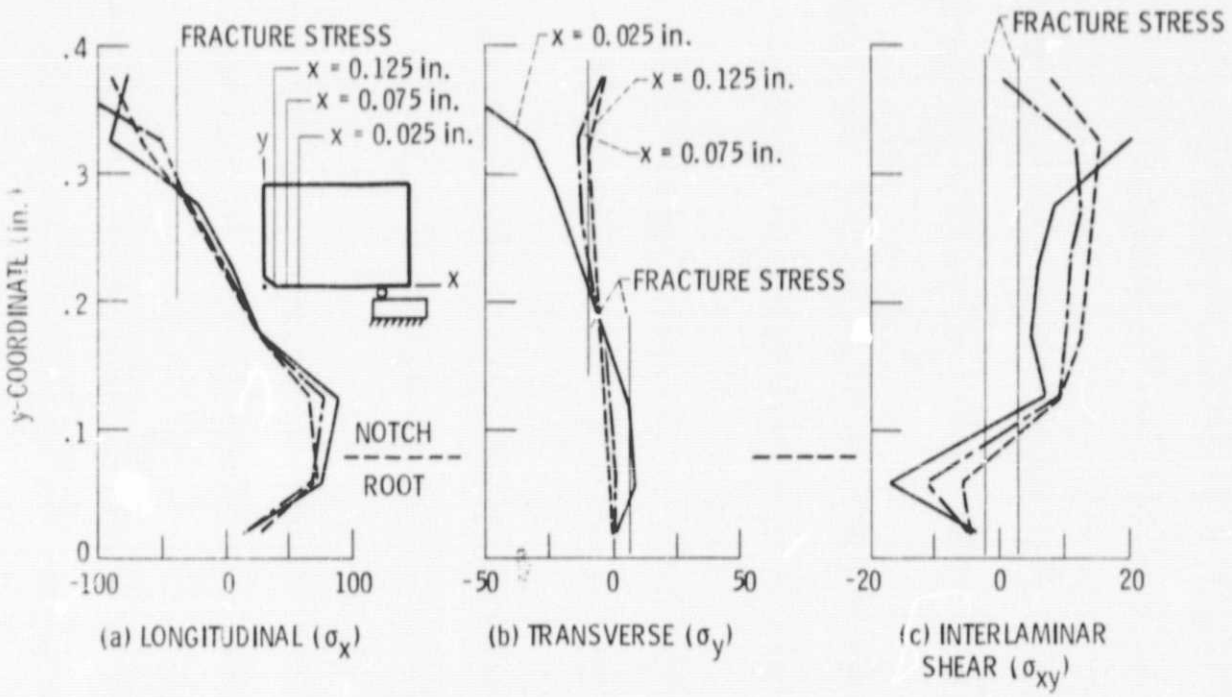

Figure 5. - KEV 49/E ASTM Charpy test specimen: variation of stresses at sections in the vicinity of notch (static load = 1341 lb).

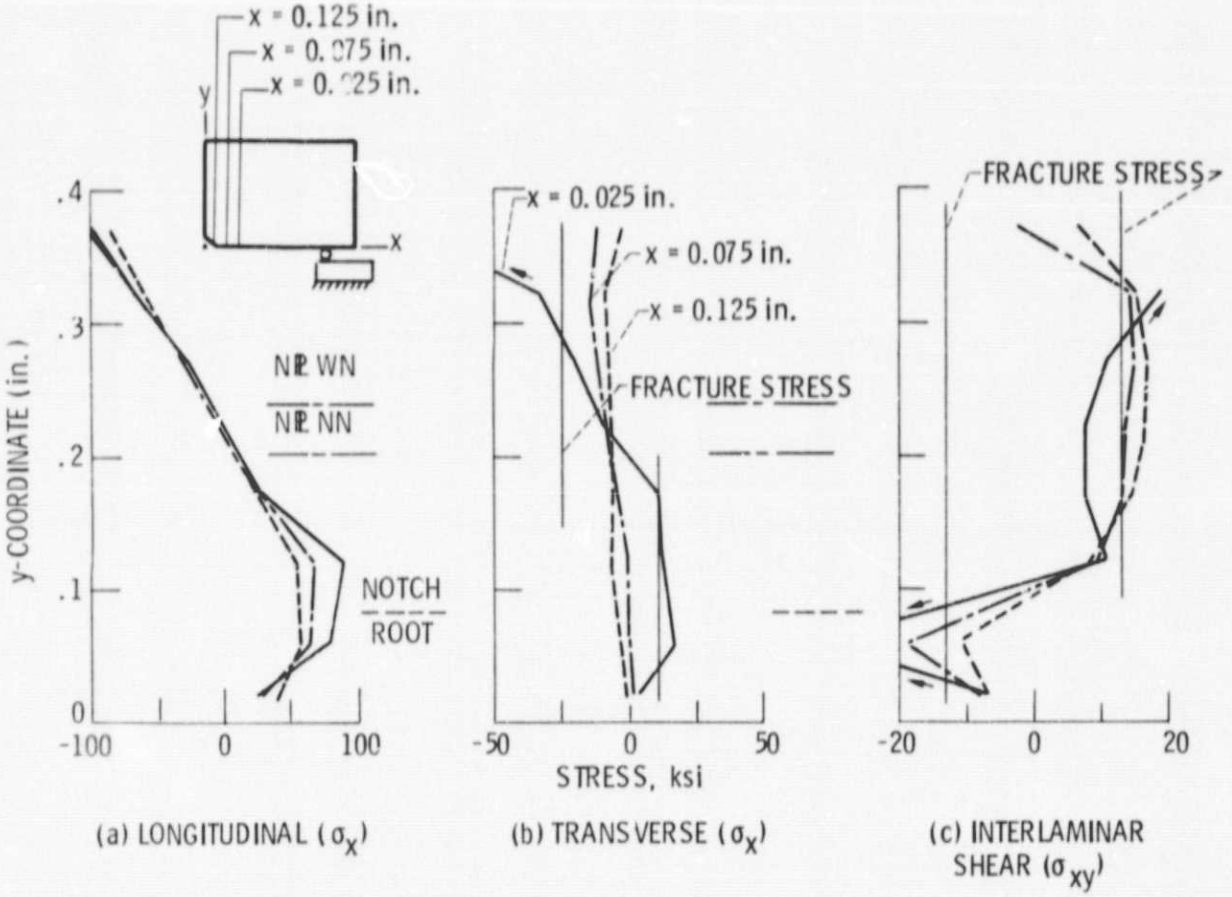

Figure 6. - S-GL/E ASTM Charpy test specimen: variation of stresses at sections in the vicinity of notch (static load = 2640 lb).

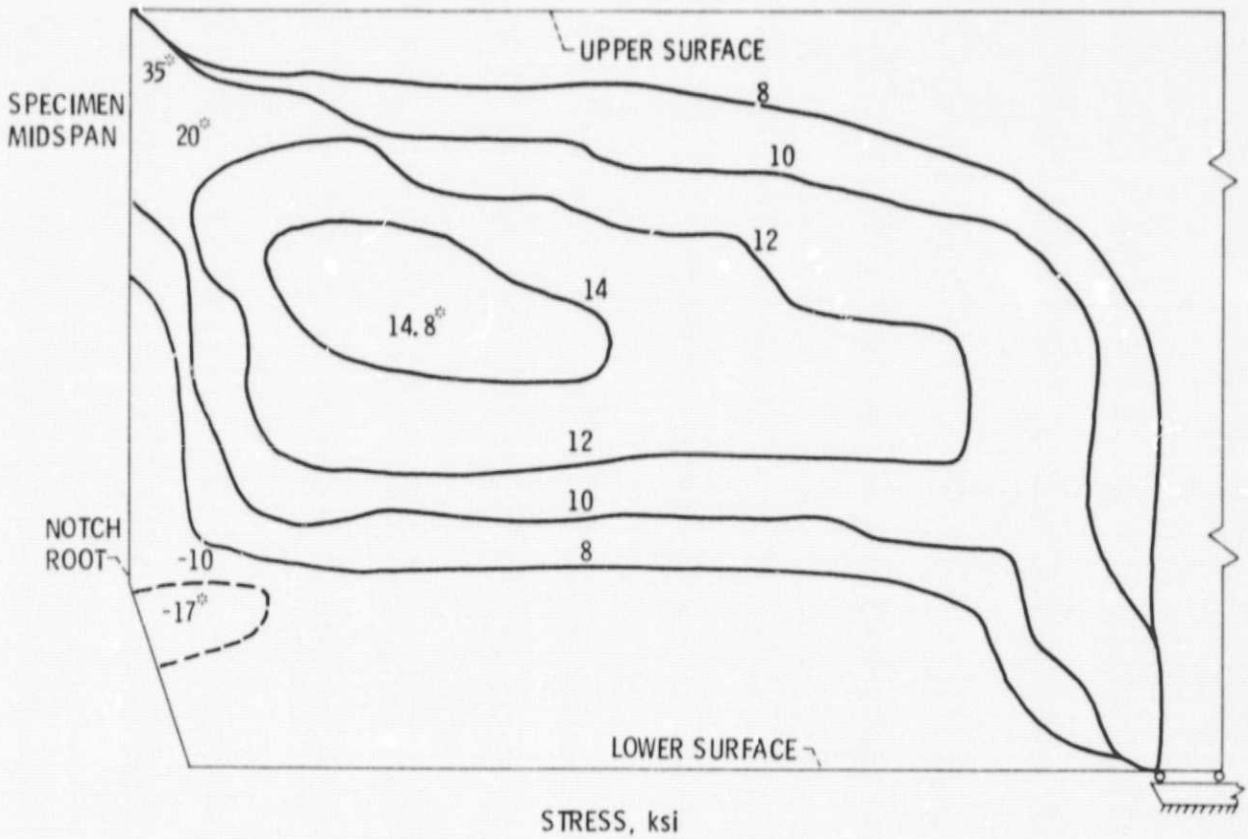

Figure 7. - KEV 49/E ASTM Charpy test specimen: interlaminar shear stress contours through the specimen thickness (static load = 1341 lb). (* denotes peak stress within contour.)

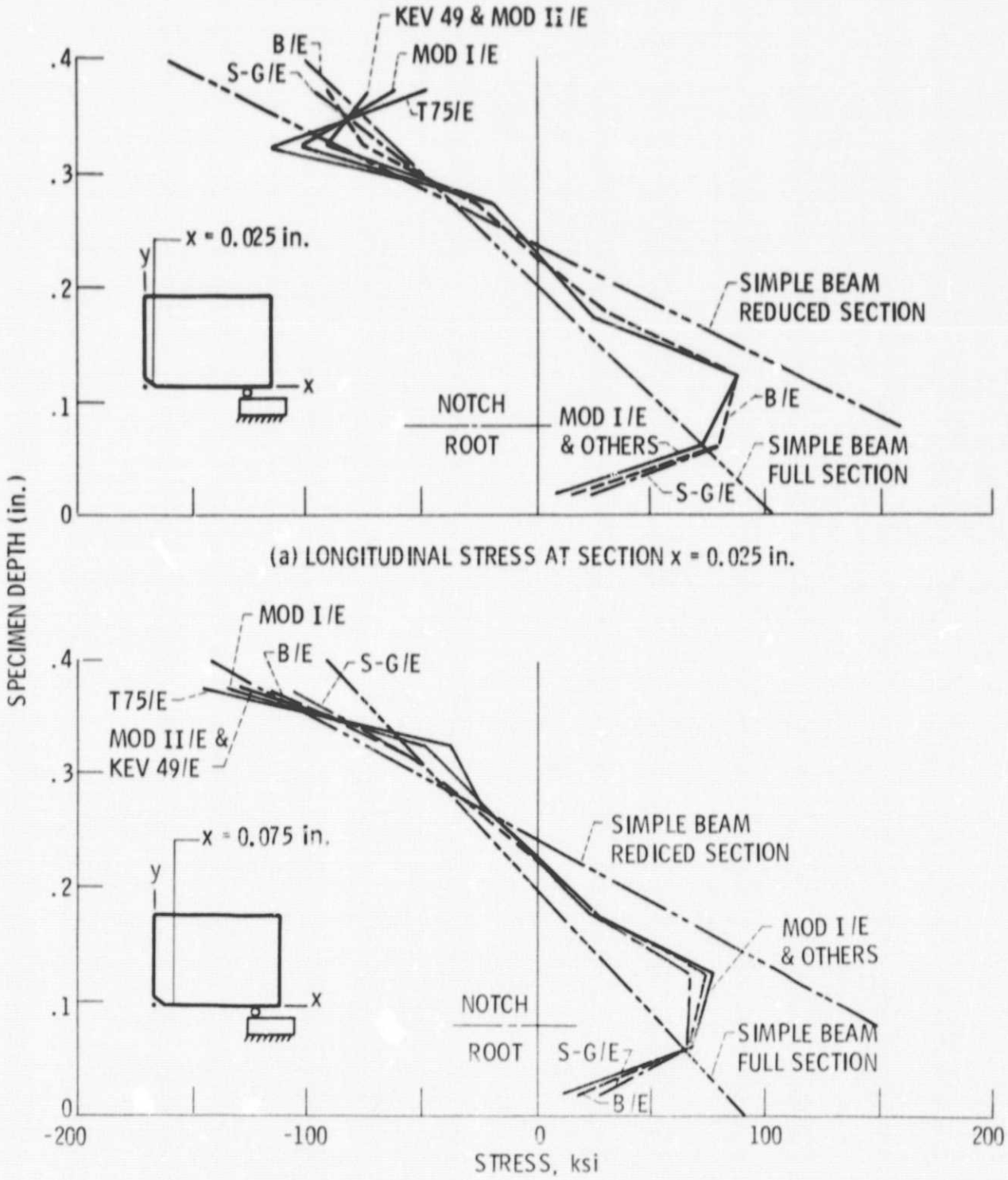

(a) LONGITUDINAL STRESS AT SECTION x = 0.025 in.

(a) LONGITUDINAL STRESS AT SECTION x = 0.075 in.

Figure 8. - Longitudinal stress variation in the notch vicinity of ASTM Charpy composite test specimens and comparisons with simple beam predictions (static load = 1320 lb).

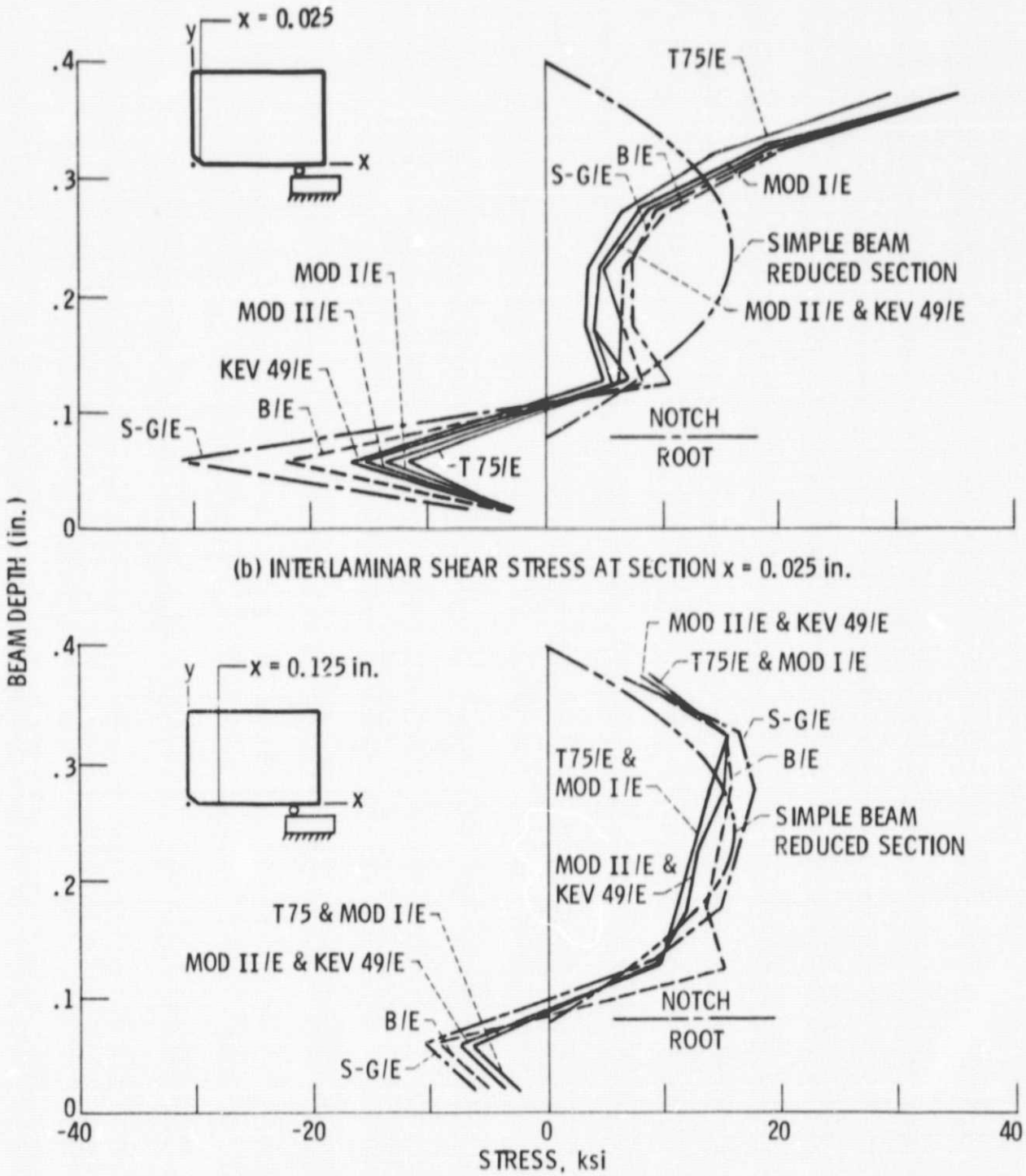

(b) INTERLAMINAR SHEAR STRESS AT SECTION x = 0.025 in.

(b) INTERLAMINAR SHEAR STRESS AT SECTION x = 0.125 in.

Figure 9. - Interlaminar shear stress variation in the notch vicinity of ASTM Charpy composite test specimens and comparisons with simple beam predictions (static load = 1320 lb).

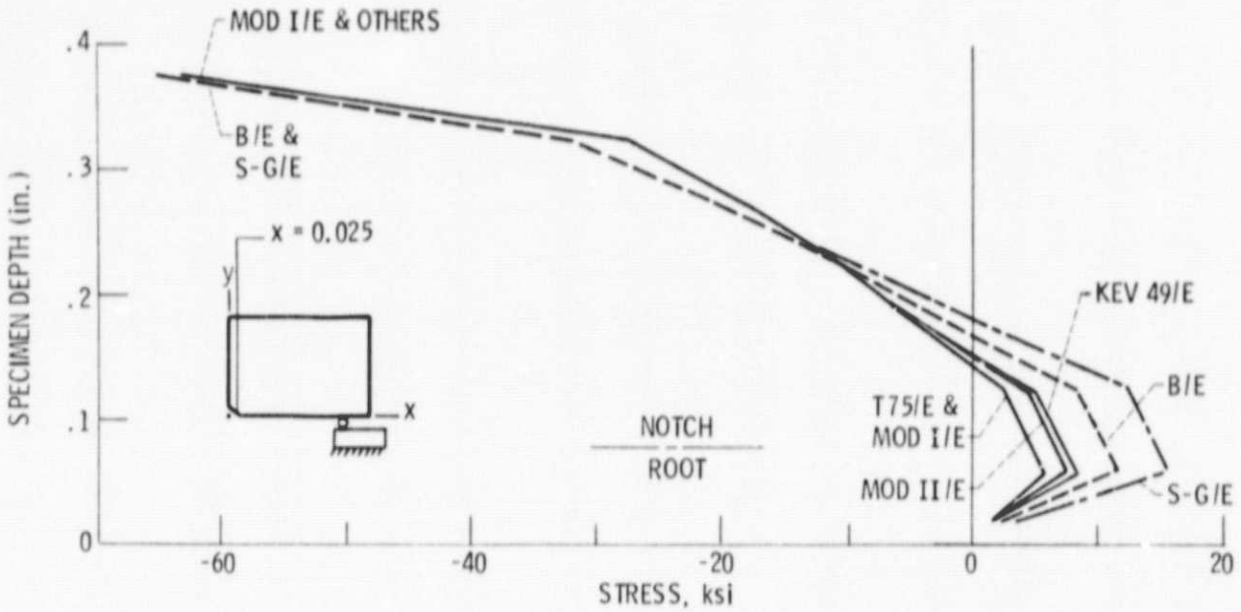

Figure 10. - Through-the-thickness normal stress variation in the notch vicinity of ASTM Charpy composite test specimens at section x = 0.025 in. (static load = 1320).

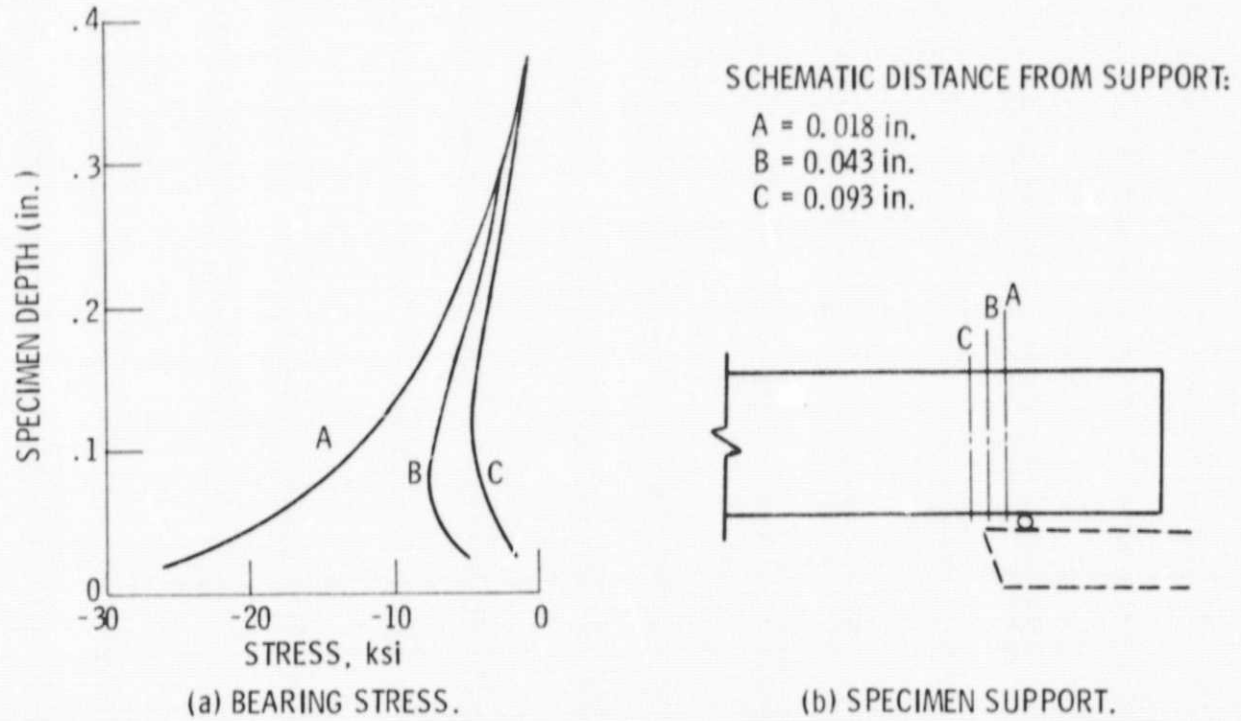

(a) BEARING STRESS.

(b) SPECIMEN SUPPORT.

Figure 11. - Typical bearing stress variation in the vicinity of the support of ASTM Charpy composite test specimens (static load = 1320 lb).

NASA-Lewis